Coherent elliptic states in lithium

K.S. Mogensen, J.C. Day,* T. Ehrenreich, E. Horsdal Pedersen, and K. Taulbjerg
Institute of Physics and Astronomy, Aarhus University, DK-8000 Aarhus C, Denmark
(Received 30 November 1994)

A detailed comparison between experimental lifetimes for Rydberg atoms formed by the adiabatic crossed-field method and corresponding theoretical lifetimes has been performed to document that the crossed-field method indeed may be used to generate and control coherent elliptic states of highly excited Rydberg atoms. It is found that core effects play a negligible role except for states of very high eccentricity.

PACS number(s): 32.80.Rm,32.70.Cs,32.70.Fw,31.50.+w

I. INTRODUCTION

The adiabatic switching method for atomic beams in crossed electric and magnetic fields [1–3] has previously been used to form atoms in circular states [4,5]. Briefly, the atomic beam is first exposed to a suitably tuned multiphoton process in a region with a strong dominance of the electric field to populate the so-called linear state, i.e., the most strongly polarized Stark state of a selected Rydberg manifold. Subsequently, this state is transformed adiabatically into a circular state when the atoms pass into a region where the magnetic field is dominant. Throughout the paper we shall refer to this experimental technique as the adiabatic crossed-field method (ACFM). The intermediate states pertaining to the general situation with finite electric and magnetic fields are naturally referred to as elliptic states. The directions in space of the expectation values of the angular momentum and the Runge-Lenz vectors characterizing the elliptic state are controlled by the external magnetic and electric fields, respectively. The elliptic states, including their limiting circular and linear forms, satisfy the minimum quantum fluctuations condition [1] and may accordingly also be referred to as coherent or semiclassical states [6].

Several methods of producing Rydberg atoms in states of high angular momentum have been suggested and used [7–10]. The first demonstration of the production of circular Rydberg states used the adiabatic microwave transfer method [8] which leads to aligned but not oriented states (i.e., a statistical population of the two magnetic substates $|m_l| = l = n-1$). This method is well suited for precision spectroscopy [11]. Oriented circular states may be produced in the presence of a circularly polarized microwave field by adiabatic transformation near an avoided crossing of two dressed Rydberg states of which one is accessible by resonant laser excitation and the other correlates with a circular state in the limit of vanishing microwave field [10]. To our knowledge the ACFM is the only known method which leads in a natural way to the formation of oriented coherent elliptic states.

II. COHERENT ELLIPTIC STATES

The concept of elliptic states pertains in principle to the pure Coulomb field only, but, as we shall discuss in some detail in this paper, the extension to Rydberg atoms with small quantum defects is generally a very good approximation. In this section, we first briefly review the algebraic method pertaining to the pure Coulomb field and then discuss the results of a numerical investigation of the Rydberg states of lithium.

A. Elliptic states of the Coulomb field

Using the SO(4) dynamical symmetry of the Coulomb problem [12–14] the Hamiltonian of the hydrogen atom in electric and magnetic fields can be written as (in atomic units)

$$H = -\frac{1}{2n^2} + \mathbf{\Omega}^- \mathbf{j}^- + \mathbf{\Omega}^+ \mathbf{j}^+ \tag{1}$$

when restricted to the Hilbert space of a given principal shell n. The two vectors $\mathbf{\Omega}^\pm$ are given by

$$\mathbf{\Omega}^\pm = \mathbf{\Omega}^L \pm \mathbf{\Omega}^S = \Omega^\pm \mathbf{u}^\pm \tag{2}$$

where the Larmor and Stark precession vectors $\mathbf{\Omega}^L$ and $\mathbf{\Omega}^S$ are defined by

$$\mathbf{\Omega}^L = \mu_B \mathbf{B}, \tag{3}$$

$$\mathbf{\Omega}^S = -\frac{3}{2} n \mathbf{E}, \tag{4}$$

in terms of the external electric ($\mathbf{E}$) and magnetic ($\mathbf{B}$) fields. The quantity μ_B is the Bohr magneton and $\mathbf{u}^\pm$ are unit vectors. The two operators $\mathbf{j}^\pm$ are defined in terms of the orbital angular momentum $\mathbf{l}$ and the Runge-Lenz vector $\mathbf{a}$,

*Permanent address: Department of Physics and Astronomy, University of Kentucky, Lexington, KY 40506-0055.

$$\mathbf{j}^{\pm} = (\mathbf{l} \pm \mathbf{a})/2. \tag{5}$$

The operators $\mathbf{j}^{\pm}$ represent the well-known SU(2)×SU(2) reduction of the SO(4) dynamical symmetry group of the Coulomb field and are pseudo-spin vectors within the considered principal shell [13]. As a matter of fact, $(\mathbf{j}^{+})^2$ and $(\mathbf{j}^{-})^2$ are diagonal with the same eigenvalue $j(j+1)$ with $j = (n-1)/2$, while the spectrum of $j_z^{\pm}$ is restricted to the usual set of eigenvalues, $-j \leq m^{\pm} \leq j$.

The situation is particularly simple when the electric and magnetic fields are orthogonal as assumed in the rest of this paper. Then we have $\Omega^{-} = \Omega^{+} = \Omega$ while the orientation of the two vectors may be characterized by their angle of inclination to the magnetic field

$$\alpha = \arctan\left(\frac{\Omega^S}{\Omega^L}\right) . \tag{6}$$

The energy eigenvalues of the Hamiltonian in Eq. (1) are given by

$$E = -\frac{1}{2n^2} + \Omega(m^{+} + m^{-}) \tag{7}$$

with the corresponding eigenstates

$$|jm^{-}\rangle_{\mathbf{u}^{-}} |jm^{+}\rangle_{\mathbf{u}^{+}}, \tag{8}$$

where it is noted that the two pseudo spins are quantized along different directions. We note that the eigenenergies are independent of the orientation of the vectors $\mathbf{\Omega}^{\pm}$ and never cross even when the magnitude Ω is varied. This implies that the atom develops adiabatically in the pseudo-spin product representation if the external fields are changed at a sufficiently slow rate. The state of the atom may accordingly be manipulated in a controlled way if the two external parameters α and Ω are slowly varied. In particular it is noted that the energies are unchanged if Ω is kept fixed but that the corresponding eigenstates change when the angle α is varied. The state variation induced by a slow change of α is referred to as adiabatic switching.

It is easy to see that an angular momentum state $|j, m_j = j\rangle_{\mathbf{u}}$ with maximum projection along some direction $\mathbf{u}$ generally is a minimum uncertainty state in the sense that the Heisenberg uncertainty relation is satisfied as an equality. In accordance with quantum optics, such states are called coherent states [6]. The coherent states of the hydrogen atom in orthogonal electric and magnetic fields are, accordingly,

$$|j \pm j\rangle_{\mathbf{u}^{-}} |j \pm j\rangle_{\mathbf{u}^{+}} . \tag{9}$$

Of these four states we are primarily interested in the uppermost energy eigenstates

$$|\alpha\rangle = |jj\rangle_{\mathbf{u}^{-}} |jj\rangle_{\mathbf{u}^{+}}, \tag{10}$$

which we shall refer to as the coherent elliptic state (CES). The uppermost energy eigenstate is chosen because it appears to be much better suited for the adiabatic switching method when Rydberg atoms other than hydrogen are considered. This is further discussed in the next section.

The α parameter is controlled by the ratio between the E and B fields. In the weak electric-field limit, α vanishes and the two vectors, $\Omega_{\pm}$, are both directed along the magnetic field. Then, the CES is an eigenstate of $l_B = j_B^{+} + j_B^{-}$ with the z axis along $\mathbf{B}$ corresponding to $m_l = 2j = n-1$. The CES accordingly represents a state with maximum orbital angular momentum projection, i.e., a circular state. In the weak magnetic-field limit, on the other hand, $\alpha = \pi/2$, and the two vectors $\mathbf{\Omega}_{\pm}$ are parallel to the $\mathbf{E}$ field, but oppositely directed. In this case the CES is an eigenstate of the orbital angular momentum projection along the $\mathbf{E}$ field $l_E = j_E^{+} + j_E^{-}$ corresponding to $m_l = j - j = 0$ while the eigenvalue of the corresponding component of the Runge-Lenz vector $a_E = j_E^{+} - j_E^{-}$ is given by $k = -2j = -(n-1)$ which, according to standard SO(4) theory is identified as the polarization quantum number in the parabolic representation of the hydrogen atom. The CES state, accordingly, represents a Stark state with maximum polarization in the direction of the $\mathbf{E}$ field in this limiting case.

A general expansion of the CES on the spherical basis set pertaining to the considered principal shell has been derived in Ref. [1]. With reference to a quantization axis along the magnetic field the expansion reads

$$|\Psi_\alpha\rangle = \sum_{lm} c_{nlm} |\Psi_{nlm}\rangle, \tag{11}$$

where $l+m$ is even and where

$$c_{nlm} = (-1)^{\frac{l-m}{2}} \frac{2^{n-l-1}(n-1)!}{(\frac{l-m}{2})!\,(\frac{l+m}{2})!} \sqrt{\frac{(l+m)!(l-m)!(2l+1)}{(n-l-1)!(n+l)!}} \sin\left(\frac{\alpha}{2}\right)^{n-m-1} \cos\left(\frac{\alpha}{2}\right)^{n+m-1} . \tag{12}$$

These authors have also shown [1] that the corresponding expectation value of the orbital angular momentum in the direction of the $\mathbf{B}$ field is given by

$$\langle l_B \rangle_{\Psi_\alpha} = (n-1)\cos\alpha, \tag{13}$$

while the expectation value of the Runge-Lenz vector in the direction of the $\mathbf{E}$ field is given by

$$\langle a_E \rangle_{\Psi_\alpha} = (n-1)\sin\alpha. \tag{14}$$

The corresponding expression for the electric dipole moment is

$$\langle d_E \rangle_{\Psi_\alpha} = -\frac{3}{2} n(n-1)\sin\alpha. \tag{15}$$

Using the classical relations between the Runge-Lenz vector, the angular momentum, and the parameters of the elliptic orbit, we may identify $\epsilon = \sin\alpha$ as the eccentricity of the corresponding classical orbit. Explicitly, in cgs

units,

$$\epsilon = 1/\sqrt{1+\left(\frac{2.18B(\mathrm{G})}{3nE(\mathrm{V/cm})}\right)^2} \qquad (16)$$

from which the circular ($\epsilon = 0$) and Stark ($\epsilon = 1$) limits are readily identified.

B. Elliptic states of lithium atoms

The algebraic method used in the previous section is based on the dynamic symmetry of the pure Coulomb field and is accordingly directly applicable only in the case of the hydrogen atom. The question is, of course, if the results of the algebraic method may be applied as a useful approximation in the case of Rydberg atoms with a central core. This question is illuminated in the present section. For this purpose it is convenient to use quantum defect theory [15–17] to represent the atom in a one-electron model. The energy eigenvalues and the corresponding eigenstates of the atom in crossed electric and magnetic fields are then readily determined by a diagonalization of the model Hamiltonian including the Stark and Zeeman coupling terms. For sufficiently weak fields, intershell couplings may be ignored. The expansion of the eigenstates of the atom may then be restricted to the manifold of the considered principal shell. Specifically, we write the wave function for the uppermost state in the manifold in a form similar to Eq. (11)

$$\Psi_{n,E,B}(r,\theta,\phi) = \sum_{l,m} b_{lm}(E,B) R_{n^*l}(r) Y_{lm}(\theta,\phi), \qquad (17)$$

where $Y_{lm}(\theta,\phi)$ are standard spherical harmonics with respect to the magnetic-field direction and $R_{n^*l}(r)$ are quantum defect wave functions as defined by Bates and Damgaard [15]. The effective principal quantum number

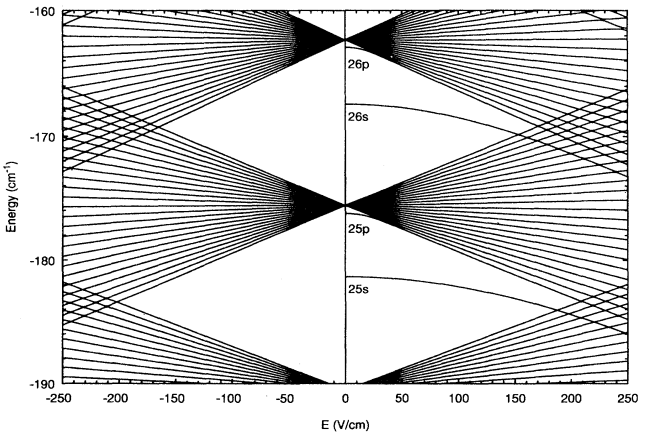

FIG. 1. Theoretical Stark spectra for hydrogen and lithium around $n = 25$ for $m = 0$. The left-hand side is the hydrogen case and the right-hand side is the lithium case. The quantum defects of the s and p states in lithium are responsible for two nonlinear Stark states below the n manifold.

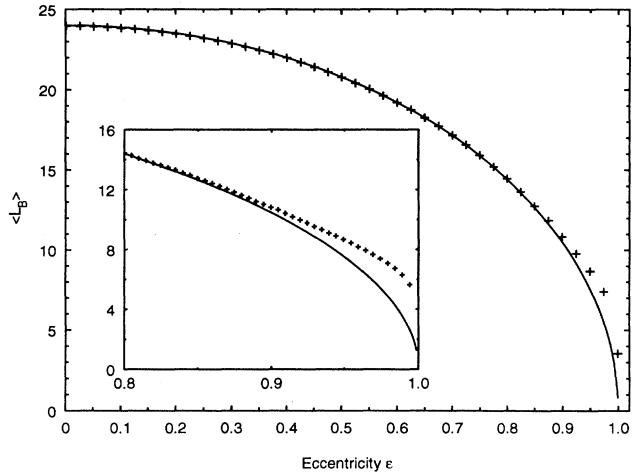

FIG. 2. The mean value of the angular momentum, Eq. (13), in the direction of the magnetic field as a function of eccentricity, Eq. (16), for a coherent elliptic state. The full curve is the Coulomb result. The crosses result from diagonalizing the quantum defect Hamiltonian for lithium for a fixed B field of 35 G.

n^* is related to the quantum defect ν_l in the usual way, $n^* = n - \nu_l$. The reader is referred to the Appendix for further details. Notice that the expansion coefficients in Eq. (17) depend on E as well as B and not only on their ratio as in the pure Coulomb case. The expansion coefficients are, however, rather similar in practical cases. It is accordingly convenient to retain the ellipticity parameter ϵ as a measure of the ratio between the field strengths and

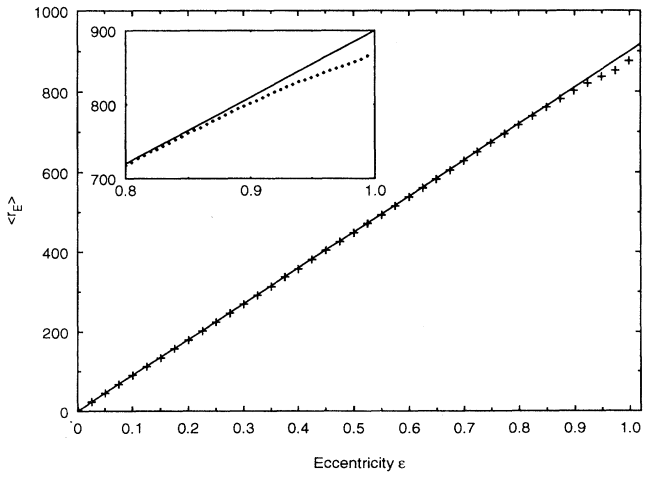

FIG. 3. The mean value of the electric dipole moment in the direction of the electric field, Eq. (15), as a function of eccentricity, Eq. (16), for a coherent elliptic state. The full curve is the Coulomb result. The crosses result from diagonalizing the quantum defect Hamiltonian for lithium for a fixed B field of 35 G.

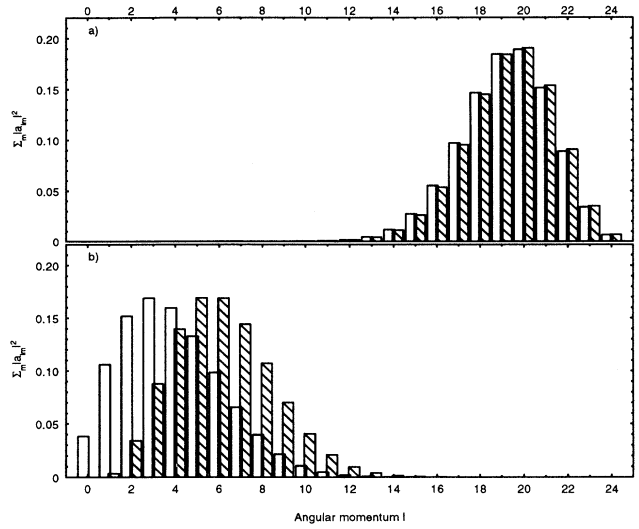

FIG. 4. The l distribution for coherent elliptic states. (a) Eccentricity $\epsilon = 0.6$; (b) $\epsilon = 0.999$. The hatched bars show quantum defect results. The empty bars show Coulomb results. The two distributions almost coincide for $\epsilon = 0.6$ but for $\epsilon = 0.999$ one notices a significant difference which is due to the quantum defects of low-l states.

allow for a weaker dependence upon the overall strength of the fields as an additional parameter to be specified in the general case.

To compare the quantum defect theory and the Coulomb theory we show in Fig. 1 the Stark spectra for hydrogen and lithium [16] for the $m = 0$ case. At strong electric fields the upper and lower states correspond to maximally polarized but oppositely directed Stark states, i.e., elliptic states with unit eccentricity. The elliptic character is preserved for both states at lower field strengths in the hydrogenic case, but for lithium the elliptic character is preserved only for the upper energy state while the lower state evolves into an s state. We have also calculated the mean value of the angular momentum in the direction of the magnetic field and the mean value of the electric dipole moment in the direction of the electric field for hydrogen and lithium in the CES state (i.e., the uppermost energy eigenstate within the considered principal shell). The case of $n = 25$ is shown in Figs. 2 and 3. For ϵ below 0.9 the average values of the electric dipole moment and the angular momentum are almost indistinguishable, whereas for higher eccentricities significant differences develop. This is reflected also in the l distributions which differ markedly for the more eccentric states as illustrated in Fig. 4.

C. Decay rates of elliptic states

The theoretical decay rates can be obtained by using the formula [18]

$$\lambda_e = \sum_{l=0}^{n-1} \sum_{m=-l}^{l} |b_{lm}(E,B)|^2 \lambda_l, \tag{18}$$

where λ_l is the decay rate for the spherical state of the angular momentum l. The b_{lm}'s are the expansion coefficients of the coherent elliptic state on a spherical basis corresponding to Eq. (17) and are to be replaced by the coefficients c_{nlm} from Eq. (12) in the pure Coulomb case. Although the elliptic state is a coherent superposition of spherical states, there are no interference terms in the total decay rate since such cross terms are readily shown to vanish identically in decay processes to isotropic manifolds of final states. The decay rates λ_l were obtained from the data of Refs. [19,20] by extrapolation from $n \leq 20$ using appropriate scaling rules. The values which we use in the present work are listed in Table I.

The lifetime $\tau_e = 1/\lambda_e$ of the CES is shown in Fig. 5. It decreases significantly with increasing ϵ corresponding to an increasing content of lower angular momentum states. This effect is independent of core effects so long as ϵ is less than 0.8 in accordance with the results of Sec. II B. For $\epsilon \geq 0.8$, however, quantum defects become increasingly important and ultimately change the lifetime by as much as a factor of 2 relative to the Coulomb case. The difference between quantum defect and Coulomb cases is large enough that it can be tested by experiments as discussed in Sec. IV B.

In practice it is difficult to avoid populating the second highest energy level in the Stark manifold by the ini-

TABLE I. Lifetimes of spherical eigenstates for lithium with principal quantum number 25.

l	τ_l (μs)
0	12.7
1	43.9
2	7.43
3	16.3
4	27.5
5	41.8
6	59.3
7	79.9
8	103.
9	130.
10	161.
11	194.
12	231.
13	271.
14	313.
15	359.
16	409.
17	461.
18	516.
19	575.
20	637.
21	703.
22	771.
23	842.
24	917.

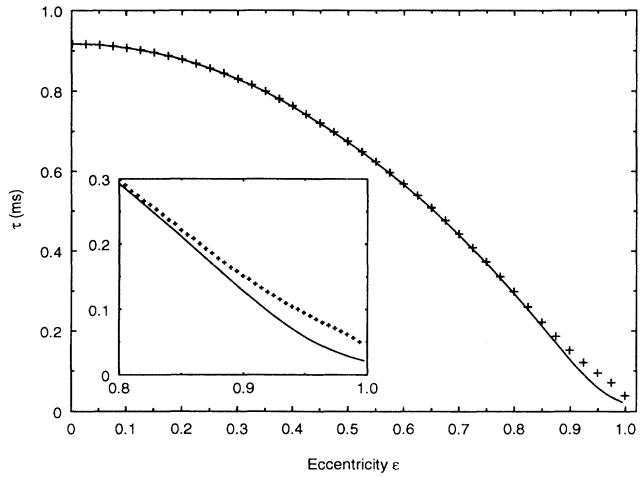

FIG. 5. Theoretical lifetime of coherent elliptic states as a function of eccentricity. Full curve, hydrogen; crosses, lithium. $B = 35$ G.

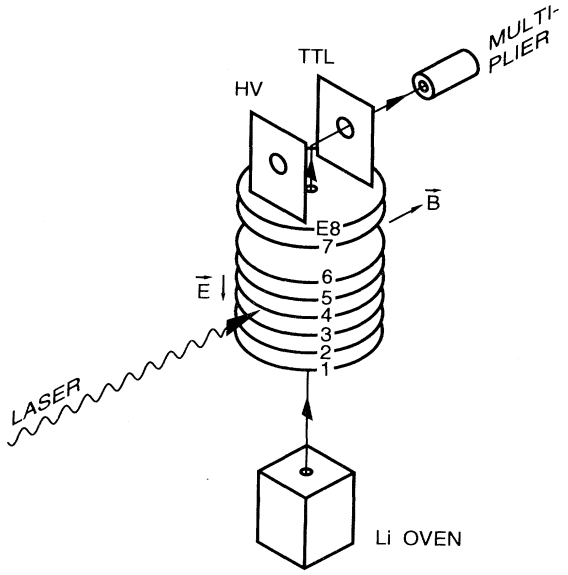

FIG. 6. Schematic diagram of the experimental arrangement showing the Li oven, the laser beams, the stack of Stark plates (E1–E8), the field ionization plates, and the detector for Li^+ ions formed by selective field ionization. The distance between Stark plates is 5 mm except for E6–E7 which is 10 mm. The distance along the Li beam from the crossing with the lasers to the region of field ionization is 50 mm. The Rydberg atoms are linear from excitation to E5, elliptic from E5 to E8, and circular from E8 to field ionization.

tial excitation process in the crossed-field method. The expansion of the corresponding eigenstates is similar to Eqs. (11) and (12) in the algebraic method and is readily identified as eigenvectors in the diagonalization method. Qualitatively, these states are very similar to the CES for high n values, and will be referred to as near-elliptic states. The decay rate for the near-elliptic states is also determined by Eq. (18) and is of some importance in our discussion (in Sec. IV A) of the elliptic purity of the ensemble of Rydberg atoms produced experimentally by the ACFM technique.

III. EXPERIMENTAL SETUP AND PROCEDURES

The experimental lifetimes for coherent elliptic Rydberg states presented here were obtained by the use of a time-of-flight technique in which the attenuation of an ensemble of elliptic Rydberg atoms of a given velocity is observed over a known distance. The most essential experimental components and procedures were described earlier [18]. For convenience we briefly discuss the main components again and add further details. A schematic drawing of the experimental setup is shown in Fig. 6. An oven loaded with a few grams of Li and electronically held at a fixed temperature T near 700 K ($\Delta T < 1$ K) emits a thermal beam of lithium atoms into the surrounding vacuum system ($\simeq 2 \times 10^{-7}$ torr) through a long circular pipe ($l = 30$ mm, $d = 3$ mm), heated to a temperature somewhat above that of the oven itself. The thermal Li beam drifts through a stack of eight circular plates E1–E8 with 3 mm holes in the center for the beam and finally into a region between two rectangular plates. Plates E1 through E4 are held at suitable potentials to form a homogeneous electric dc field of 150 V/cm parallel to the Li beam while plates E5 though E8 define a variable dc field, typically in the range 0–10 V/cm. The hole in plate E4 is covered by a fine copper grid (80% transmission) to ensure that the field in the region between plates E3 and E4 is truly homogeneous.

Between plates E3 and E4 the Li beam is crossed by three collinear laser beams which are tuned to resonance with the transitions $2s$ to $2p$ (671 nm), $2p$ to $3d$ (610 nm), and $3d$ to the uppermost Stark level of the $n = 25$ manifold (831 nm) formed by the external electric field (150 V/cm). A representative Stark spectrum is shown in Fig. 7. The uppermost state is marked by an arrow. All three lasers are dye lasers pumped by a pulsed Nd:YAG laser running at 14 Hz and with a pulse length of 5 nsec. The dye-laser beams were all linearly polarized in the direction of the electric field. The first two transitions were saturated by relatively weak and broad band laser beams (average power < 1 mW, linewidth > 10 GHz). The last transition was not saturated (average power 10 mW, linewidth 6.5 GHz). The average number of Rydberg atoms produced under these circumstances is estimated to be of the order of 10^5 atoms per shot.

After excitation the Rydberg atoms drift into the regions defined by plates E4 to E5 and E5 to E8 in which there are smaller electric fields and a crossed magnetic field (B) of the order of 50 G. In the first of these two regions the electric field is typically 20 V/cm. This is high enough that the structure of the Rydberg atoms is dominated by the electric field and they are therefore still linear in this region, but as the atoms drift through

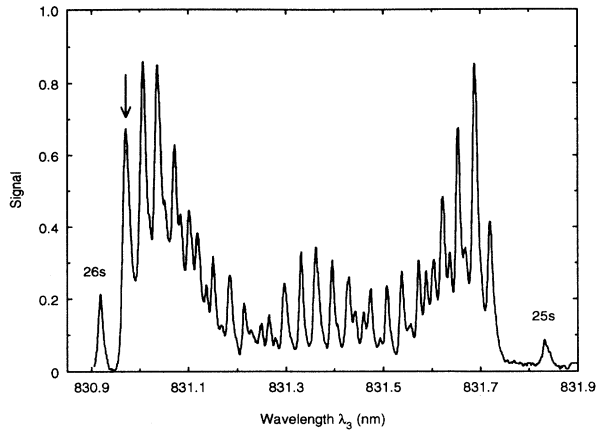

FIG. 7. Stark spectrum for $E = 150$ V/cm. Labels $26s$ and $25s$ refer to states correlating with the indicated nl states for $E = 0$. The uppermost Stark state is indicated by an arrow.

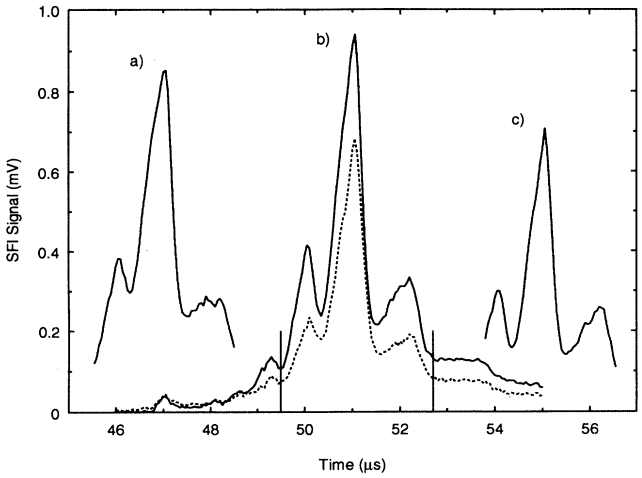

FIG. 8. Typical SFI spectra for circular Rydberg atoms. The side peaks of each spectrum are due to blackbody radiation. The spectra illustrate the influence of blackbody radiation for three delays, t_d, of the HV ramp and for two eccentricities, ϵ. (a) $t_d = 39$ μs, $\epsilon = 0$; (b) $t_d = 43$ μs, $\epsilon = 0$; (c) $t_d = 47$ μs, $\epsilon = 0$. Dotted curve: $t_d = 43$ μs, $\epsilon = 0.98$. Integration limits for spectrum (b) are indicated.

the hole in plate E5 they experience a slow (adiabatic) decrease of the electric field to a value E for which the structure of the Rydberg atoms depends on E as well as on B. In this region the Rydberg atoms are in an elliptic state with eccentricity determined by E/B [Eq. (16)]. The atoms finally drift into a region of zero electric field between the two rectangular plates arranged parallel to the beam. The plates are separated by 1 cm. One is connected to a fast pulser ($0-5$ V, rise time 5 ns), while the potential of the other is controlled by a linear high-voltage (HV) ramp generator with a typical slew rate of 300 V/μs. In this region the Rydberg atoms are circular and here they are ionized by the electric field formed by the linear HV ramp which is normally started 43 μs after the laser pulse. The other plate (TTL in Fig. 6) as well as the last circular plate E8 are at ground potential except that a small voltage in the form of TTL pulse (transistor transitor logic) is applied to the rectangular plate TTL when the HV is on. This field stabilizes the circular state at the beginning of the ramp (see Ref. [4]). The ionized Rydberg atoms are accelerated by the ramp field onto a secondary electron multiplier through a hole in the plate at low potential. The multiplier output is recorded by a digital oscilloscope. The resulting spectrum is a selective field ionization (SFI) spectrum [21,22].

Typical SFI spectra are shown in Fig. 8 for *parallel* magnetic and electric fields. In each spectrum the center peak corresponds to a circular state with $n = 25$ whereas the two side peaks are due to blackbody radiation-induced high l states with $n = 24$ and $n = 26$. Traces of atoms with higher and lower n values are also seen. All material surrounding the beam was cooled by liquid nitrogen to reduce transitions between Rydberg states induced by the blackbody radiation. The remaining redistribution of Rydberg states due to blackbody radiation may change when the eccentricity or the delay for the HV ramp is varied. The spectrum labeled (b) and the dotted one in Fig. 8, taken under standard experimental conditions, illustrate the dependence on eccentricity which is clearly weak. The dependence on delay is illustrated by spectra (a), (b), and (c). A shorter delay results in a reduced redistribution due to the shorter exposure to blackbody radiation. Under standard experimental conditions the Rydberg atoms have been exposed to the blackbody radiation for only about 18 μs near the center of the elliptic region (E5–E8). The redistribution in this region is therefore somewhat smaller than seen even in spectrum (a). The areas are measures of the total number of atoms in the given states. The diversion by blackbody radiation may be effectively compensated for by taking the area of the three central peaks as a measure of the number of surviving Rydberg atoms in the elliptic state.

The experiment determines a survival fraction defined as the ratio between the SFI area measured for $E \neq 0$ and $E = 0$, where E is the electric field in the region E5–E8 where the Rydberg atoms are in an elliptic state. The survival fraction for an elliptic state is given by [18]

$$R_{e/c} = \exp\left(-[\lambda(E,B) - \lambda(0,B)]\frac{L_{III}}{L}\Delta t\right) \qquad (19)$$

where the quantities $\lambda(E,B)$ and $\lambda(0,B)$ are the decay rates of the elliptic state and a circular state, respectively, L_{III}/L is the ratio between the length of the region where the atoms are in an elliptic state L_{III} and the length of the total drift region L, and Δt is the time interval from excitation to field ionization. The time $(L_{III}/L)\Delta t$ spend by the atoms in the elliptic state was typical 20 μs. The survival fraction (19) was determined as a function of E by recording SFI spectra for a series of E's. Each

spectrum was preceded and followed by a spectrum for $E = 0$, and the ratio between the area of the spectrum and the average of the two normalization spectra was calculated. The measurements were performed automatically under the control of a personal computer. To get a measure of the statistical fluctuations of the measured survival fractions we measured each point a number of times (typically ten) and calculated the standard deviation.

The effective length of the region L_{III} was determined by

$$L_{III} = \frac{\int[\lambda(E,B) - \lambda(0,B)]x dx}{\int[\lambda(E,B) - \lambda(0,B)]dx}, \tag{20}$$

where the integration is along the beam direction and $E(x)$ is found by solving Poisson's equation in the region between electrodes E5 and E8 for typical voltages. The L_{III} value depends on the voltage and the distance from the center axis. The variation is small (≤ 1 mm) compared to the average value of 20.5 mm. The total drift length L was 50 mm.

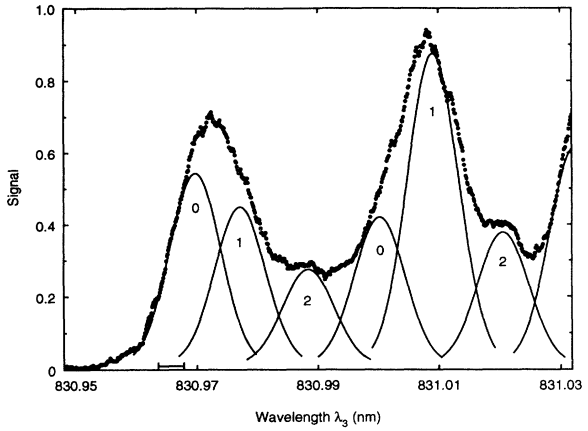

FIG. 9. Partial Stark spectrum of lithium obtained by scanning the wavelength λ_3 of the third laser. Stark field $E_s = 150$ V/cm, $B = 35$ G. The uppermost states (in energy) are resolved into individual $|m_l| = 0$, 1, and 2 lines. The range of λ_3 values near 830.966 nm for which pure elliptic states may be formed is indicated.

IV. RESULTS AND DISCUSSION

A. Purity of initial Stark ensemble

The uppermost state of the Stark manifold for a given shell is the starting point of the adiabatic switching process and has orbital angular momentum $m_l = 0$ along the direction of the external electric field $\mathbf{E}_S$. According to our previous discussion this state is denoted by $\Psi_{\alpha=\pi/2}$ and corresponds to the CES with maximum eccentricity, $\epsilon = 1$. The three laser beams are all linearly polarized parallel to the Stark field $\mathbf{E}_S$. The dipole selection rule for this polarization, $\Delta m_j = 0$, where $m_j = m_l + m_s$ is the total angular momentum quantum number and m_s is the spin projection of the active electron, allows excitation of the initial state with $|m_j| = \frac{1}{2}$ to Stark states with $m_l = 0$ and $|m_l| = 1$, where the last possibility is due to spin-orbit mixing. In the presence of a crossed magnetic field, $\mathbf{B}$, the quantities, m_j, m_l, and m_s are strictly speaking no longer good quantum numbers but when $\mathbf{B}$ is sufficiently small that the paramagnetic Zeeman coupling can be treated as a perturbation, the effect of the B field is to couple unperturbed $|m_l| = 1$ states with $m_l = 0$ and $|m_l| = 2$ states. The excitation of Stark states with $|m_l| \leq 2$ is thus allowed by the dipole selection rule. In hydrogen the $\Psi_{\alpha=\pi/2}$ state is nondegenerate and may therefore be excited selectively if the bandwidth of the appropriate laser is sufficiently narrow. The same applies to Li but the quantum defect of the $m_l = 0$ states results in an energy separation of only about 4 GHz between the uppermost $m_l = 0$ and $|m_l| = 1$ states. This is relatively small as compared to the linewidth (6.5 GHz) of the third laser driving the last transition and prevents a clear spectral separation of the two uppermost Stark states. Figure 9 shows a detailed excitation spectrum illustrating this. Each structure in the spectrum has been resolved into 3 lines with $m_l = 0, 1$, and 2 as indicated in the figure. It is apparent from the figure that the admixture of $|m_l| \geq 1$ states is effectively suppressed when the laser is detuned a few GHz towards smaller wavelengths. This is substantiated in the next section.

B. Experimental and theoretical survival fractions

The survival fraction of the experimental Rydberg ensemble depends on the wavelength, λ_3, of the third laser, the ratio E/B of the Stark and Zeeman fields, and the absolute strengths of the fields. We shall now discuss this dependence and compare experimental and theoretical results.

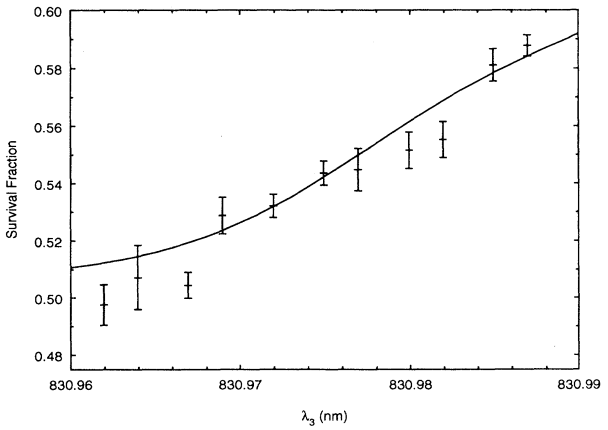

FIG. 10. Survival fraction as a function of wavelength λ_3 of the third laser for $\Delta t = 51$ μs, $E_s = 150$ V/cm, $E = 70$ V/cm, and $B = 35$ G. The full curve is a quantum defect theoretical prediction taking into account the width of the laser and the oscillator strengths of the transitions.

1. Dependence on λ_3

The survival fraction is shown in Fig. 10 as a function of wavelength λ_3 in a situation where the eccentricity is very large such that adiabatic switching essentially has been avoided. The theoretical curve is calculated on the basis of a population distribution corresponding to the decomposition shown in Fig. 9 and on theoretical lifetimes from the quantum defect theory of Sec. II B. The consistency with the data throughout the full range of wavelengths is a strong indication that the decomposition of the initial population of Stark states is properly represented in our procedure. In particular, we note the fine agreement in the range of blue detunings where a single $m = 0$ component is isolated in Fig. 9. This provides strong evidence that the maximally polarized Stark state, i.e., the CES with $\epsilon = 1$, indeed may be exclusively populated by a suitable tuning of the laser fields.

2. Dependence on E and B

Figure 11 shows the dependence of the survival fraction on the field ratio E/B for two values of the magnetic field. The electric field $\mathbf{E}$ defining the eccentricity of the elliptic states is parallel to the Stark field $\mathbf{E}_S$ for positive E/B and antiparallel for negative E/B. The field variations seen by the Li atoms are therefore somewhat faster for negative than for positive E/B in the critical region near plate E5 (see Fig. 6) where the switching process takes place. The symmetry of the experimental data around $E/B = 0$ therefore shows that the switching process is indeed adiabatic in both cases. The experimental results and the theoretical predictions of the quantum defect theory are in good agreement and they show clearly that the survival fraction depends primarily on the field ratio but also to a smaller degree on the absolute values of the fields. The hydrogenic results deviate substantially from the measurements for $E/B > 0.2$ (V/cm)/G corresponding to eccentricities $\epsilon > 0.9$. This deviation reflects the fact that low angular momentum components are represented in different proportions for high eccentricities as already discussed in Sec. II B in connection with Fig. 4.

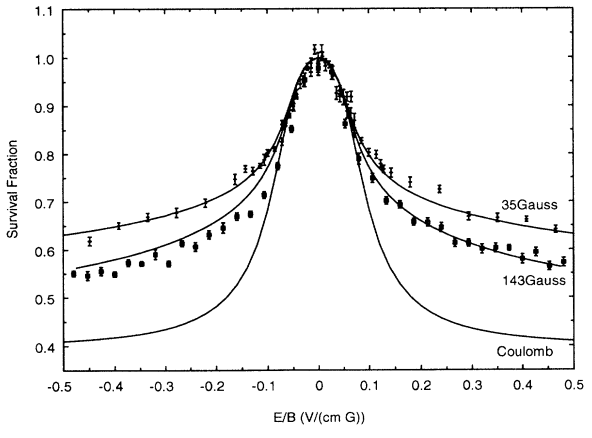

FIG. 11. Survival fractions as function of field ratio E/B for constant B fields and $\lambda_3 = 830.968$ nm and $\Delta t = 52$ μs. The two sets of data points were measured at B fields of 35 and 143 G, respectively. The corresponding theoretical curves are based on the quantum defect representation of the coherent elliptic state. For comparison the common theoretical curve based on the pure Coulomb representation is also shown.

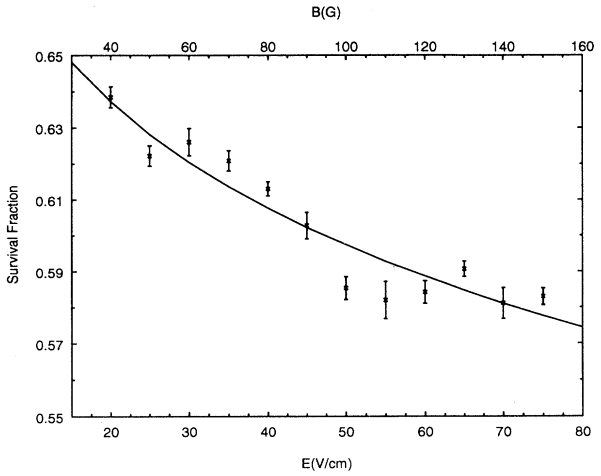

FIG. 12. Survival fraction as function of E for constant $E/B = 0.5$ V/cm/G, $\lambda_3 = 830.968$ nm, and $\Delta t = 50$ μs. The full curve shows the result of the quantum defect theory. For a purely hydrogenic system, the survival fraction is 0.41.

3. Dependence on E

The relatively weak dependence of the survival fraction on the absolute values of the fields for a constant field ratio E/B is shown in Fig. 12. The agreement between the experimental data and the quantum defect results is good whereas the hydrogenic theory clearly underestimates the survival fraction and fails to reproduce the dependence on the field strengths.

4. Dependence on ϵ

The survival fraction for coherent elliptic Rydberg atoms is shown as a function of eccentricity ϵ in Fig. 13. The survival fraction is nearly constant for smaller values of ϵ. This is due to the long lifetime of such states and the short flight path (2 cm) of the considered Rydberg atoms. The variation is, however, very pronounced in the eccentricity range above 0.6. The experimental data set is, in general, in fine accord with the theoretical results based on the quantum-defect treatment of the Rydberg manifold while there is a consistent departure from the results of the group-theoretical approach when the eccentricity becomes large. This departure is clearly due

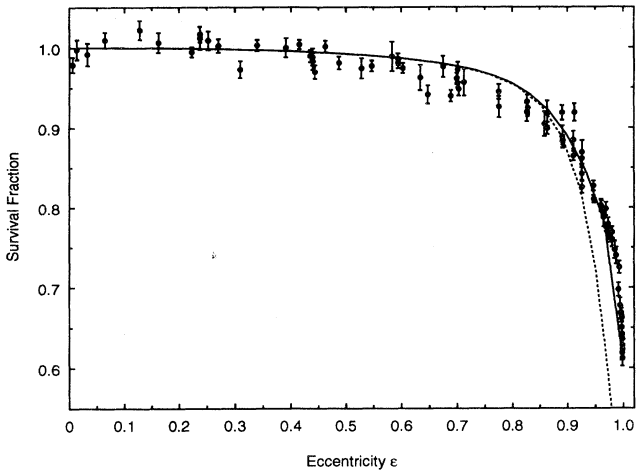

FIG. 13. Survival fraction as function of eccentricity ϵ for $B = 35$ G, $\lambda_3 = 830.968$ nm, and $\Delta t = 52$ μs. The full curve shows theoretical result of the quantum defect theory. The broken curve shows the pure Coulomb prediction.

to the fact that low angular momentum components are over represented when the Coulombic theory is applied to atoms with a central core.

C. Validity of the adiabatic crossed-field method

The accurate agreement between experimental survival fractions and corresponding theoretical results pertaining to the ideal coherent elliptic state which presumably would be populated by the adiabatic switching method in crossed electric and magnetic fields provides strong evidence that the present experimental technique can be generally used to form and control such states. The present experimental arrangement has allowed a specially critical test of strong variations of the lifetime of Rydberg states in the eccentricity range above about 0.6. The excellent agreement between theory and experiment in this critical region we take as evidence that coherent elliptic states indeed are formed by the present method. The present test is less sensitive in the region of smaller eccentricities, but we have no reason to doubt that pure and well-defined coherent elliptic states with smaller values of the eccentricity parameter can be formed by the present experimental technique as well [4] .

V. CONCLUSION

The main emphasis of the present work has been a combined experimental and theoretical study of lifetimes of Rydberg atoms formed by the adiabatic crossed-field method (ACFM). The accurate agreement between theory and experiment provides strong evidence that the ACFM indeed may be used in practice to form and control a special class of highly excited Rydberg atoms, normally refered to as coherent elliptic states (CES). The CES terminology strictly pertains only to the case of hydrogen since it is based upon the dynamic symmetry of the Coulomb field, but our studies have documented that the extension to embrace highly excited states of Rydberg atoms such as lithium is very useful from a conceptual point of view. Indeed, we have found that the states that are formed by the ACFM in lithium are very similar to those that would be formed under the same conditions in hydrogen so long as the most eccentric states are excluded. Deviations in the distribution over angular momentum states, for example, are not significant until the eccentricity ϵ of the considered state reaches a value of about 0.9. Low angular momentum states and, accordingly, core penetration effects, play an increasing role for such states. In fact, such states can no longer be strictly characterized by the eccentricity parameter but depend in addition upon the strength of the external fields. The variation is, however, rather modest and is not expected to have a significant effect unless a quantity especially sensitive to the content of low angular momentum states is at focus. The lifetime of the CES is an example where the content of low angular momentum states is tested very critically since most of the radiative decay is controlled by these states. It is therefore very pleasing that we have been able to demonstrate that the experimental lifetime of lithium Rydberg states formed by the adiabatic crossed-field method is in good agreement with theory when properly accounting for core penetration effects.

ACKNOWLEDGMENT

This work was supported by the National Science Foundation under Grant No. INT-91117374.

APPENDIX

The quantum defect wave functions have previously been described in Refs. [15–17]. In our special case the wave functions are needed to evaluate the matrix elements of the Stark Hamiltonian. The wave functions are given by

$$R_{n^*l} = \sum_{v=0}^{n-l-1} a_v r^{n-1-v} \exp\left(\frac{-r}{n^*}\right), \tag{A1}$$

where $n^* = n - v_l$ is the effective quantum number. The sequence of expansion coefficients a_v is determined by the recursion formula

$$a_v = -a_{v-1}\frac{n^*}{2}\frac{(n^* - l - v)(n^* - v + l + 1)}{v} \tag{A2}$$

and by overall normalization. In the present applications for lithium in the $n = 25$ principal shell we assume that the quantum defects vanish for $l \geq 3$ and are given by 0.3999, 0.047, and 0.002 for the s, p, and d states, respectively.

We have used the quantum defect wave functions to calculate the eigenvalues and eigenvectors for lithium in crossed fields within the $n = 25$ manifold. The calculations are valid for electric fields less than 150 V/cm. For larger fields it would be necessary to take intershell mixing into account. The magnetic field was so small ($B < 150$ G) that it was quite safe to neglect the paramagnetic term.

[1] A. Bommier, D. Delande, and J.C. Gay, *Atoms in Strong Fields*, edited by C.A. Nicolaides *et al.* (Plenum, New York, 1990).

[2] D. Delande and J.C. Gay, Europhys. Lett. **5**, 303 (1988).

[3] J.C. Gay, D. Delande, and A. Bommier, Phys. Rev A **39**, 6587 (1989).

[4] J. Hare, M. Gross, and P. Goy, Phys. Rev. Lett. **61**, 1938 (1988).

[5] S.B. Hansen, T. Ehrenreich, E. Horsdal Pedersen, K.B. MacAdam, and L.J. Dube, Phys. Rev. Lett. **71**, 1522 (1993).

[6] R.J. Glauber, Phys. Rev. **130**, 2529 (1963).

[7] M.G. Littman, M.L. Zimmerman, T.W. Duncan, R.R. Freeman, and D. Kleppner, Phys. Rev. Lett. **36**, 788 (1976).

[8] R.G. Hulet and D. Kleppner, Phys. Rev. Lett. **51**, 1430 (1983).

[9] W.A. Molander, C.R. Stroud, Jr., and J.A. Yeazell, J. Phys. B **19**, L461 (1986).

[10] C.H. Cheng, C.Y. Lee, and T.F. Gallagher, Phys. Rev. Lett. **73**, 3078 (1994).

[11] See, i.e., J. Hare, A. Nussenzweig, C. Gabbenini, M. Weidemuller, P. Goy, M. Gross, and S. Haroche, IEEE Trans. Instrum. Meas. **42**, 331 (1993).

[12] D. Park, Z. Phys. **159**, 155 (1960).

[13] M.J. Englefield, *Group Theory and the Coulomb Problem* (Wiley, New York, 1972).

[14] Yu. N. Demkov, B.S. Monozon, and V.N. Ostrovski, Zh. Eksp. Teor. Fiz. **57**, 1431 (1969) [Sov. Phys. JETP **30**, 775 (1970)].

[15] D.R. Bates and A. Damgaard, Proc. Trans. R. Soc. **242**, 101 (1949).

[16] M.L. Zimmerman, M.G. Littman, M.M. Kash, and D. Kleppner, Phys. Rev. A **20**, 2251 (1979).

[17] O.G. Larsen and K. Taulbjerg, J. Phys. B **17**, 4523 (1984).

[18] J.C. Day, T. Ehrenreich, S.B. Hansen, E. Horsdal Pedersen, K.S. Mogensen, and K. Taulbjerg, Phys. Rev. Lett. **72**, 1612 (1994).

[19] C.E. Theodosiou, Phys. Rev. A **30**, 2881 (1984).

[20] A. Lindgaard and S.E. Nielsen, At. Data Nucl. Data Tables **19**, 533 (1977).

[21] R.J. Damburg and V.V. Kolosov, J. Phys. B **12**, 2637 (1979).

[22] T.H. Jeys, G.W. Foltz, K.A. Smith, E.J. Beiting, F.G. Kellert, F.B. Dunning, and R.F. Stebbings, Phys. Rev. Lett. **44**, 390 (1980).